Federated-Learning-Assisted RIS Active and Passive Beamforming with ADMM for IoT Devices

Yujun Cai, Shufeng Li, Jianbo Liu, Qianyun Zhang, Zhijin Qin, Xinruo Zhang

Abstract-Federated learning (FL) and reconfigurable intelligent surfaces (RIS) are pivotal technologies for future Internet of Things (IoT) networks, enhancing user privacy and system efficiency. However, realizing their full potential necessitates a cohesive and synergistic integration, challenging the traditional view of them as disparate components. This paper tackles the complex problem of maximizing energy efficiency (EE)—a critical vet under-explored metric insuch tightly coupled FL-RIS systems. We address this gap by formulating ajoint optimization problem that intrinsically links the FL process with physical layer resource allocation. Our framework maximizes the system's global EE by concurrently designing the base station's active beamforming and the RIS's passive phase shifts, with an FL aggregation mechanism that is explicitly channel-aware and adaptive to the RIS-optimized wireless environment. This codesign ensures RIS actively facilitates FL by establishing robust communication, while FL intelligently leverages these improved channels for efficient and accelerated learning, all under practical FL performance constraints. Simulation results demonstrate that our proposed framework significantly enhances system energy efficiency compared to several benchmark schemes and exhibits robust convergence properties.

Index Terms—Communications and networking for IoT; federated learning; reconfigurable intelligent surface; beamforming and efficient communications

I. Introduction

The proliferation of Internet of Things (IoT) devices challenges wireless networks to deliver both high throughput and superior energy efficiency. Reconfigurable intelligent surfaces (RIS) have emerged as a key 6th generation (6G) technology to address these demands by intelligently reconfiguring the wireless propagation environment [1]. The potential of RIS has been demonstrated in diverse applications, from enhancing physical layer security and enabling non-orthogonal multiple access (NOMA) to optimizing multiple-input multiple-output

This work was supported by the National Natural Science Foundation of China No.62371428, the Fundamental Research Funds for the Central Universities No. CUC25QT16, and the Royal Society International Exchanges 2023 under Grant No. IEC\NSFC\233318 (Corresponding author: Qianyun Zhang.)

Yujun Cai, Shufeng Li, and Jianbo Liu are with the School of Information and Communication Engineering, Communication University of China, Beijing 100024, China (e-mail: tangentchase@cuc.edu.cn; lishufeng@cuc.edu.cn; ljb@cuc.edu.cn).

Qianyun Zhang is with the School of Cyber Science and Technology, Beihang University, Beijing 100191, China (e-mail: zhangqianyun@buaa.edu.cn). Zhijin Qin is with the Department of Electronic Engineering, Tsinghua University, Beijing 100084, China (e-mail: qinzhijin@tsinghua.edu.cn).

Xinruo Zhang is with the School of Computer Science and Electronic Engineering, University of Essex, Colchester CO4 3SQ, United Kingdom (e-mail: xinruo.zhang@essex.ac.uk).

© 2025 IEEE. Personal use of this material is permitted. However, permission to use this material for any other purposes must be obtained from the IEEE by sending a request to pubs-permissions@ieee.org.

(MIMO) communications [2-4]. Central to unlocking these benefits is the precise design of the RIS phase shifts, underscoring the critical role of effective beamforming techniques.

A primary focus of RIS research is the joint design of active beamforming at the base station (BS) and passive beamforming at the RIS to optimize system performance. Foundational work established key principles, such as analyzing the performance gains relative to the number of RIS elements and investigating baseline random beamforming strategies [5-6]. More recent studies propose sophisticated joint optimization algorithms. For example, some approaches maximize system throughput using statistical channel state information (CSI), while others aim to reduce computational complexity for a single-user system's spectral efficiency by decoupling the active and passive beamforming design [7-8]. Although these studies provide valuable insights, their primary focus remains on traditional spectral efficiency or throughput metrics. Furthermore, RIS is being integrated into more complex applications like over-the-air computing and high-altitude communication, which highlights the need for new beamforming designs tailored to the unique performance objectives of such emerging paradigms [9-10].

Building upon foundational beamforming techniques, recent research has increasingly focused on joint optimization frameworks that integrate RIS with other system components to address more complex communication challenges. An et al. [11] developed a low-complexity framework for simultaneous channel estimation and passive beamforming in RISassisted MIMO systems, significantly enhancing achievable rates through optimized reflection coefficients. In [12], a refracting RIS-aided hybrid satellite-terrestrial relay system was proposed to overcome signal blockage, where an alternating optimization framework based on singular value decomposition and penalty methods was developed to minimize the total transmit power while satisfying user rate requirements. For multi-RIS scenarios, Ma et al. [13] presented a cooperative beamforming design that models and decouples complex channel interactions to optimize user sum rates. Security concerns in IoT networks have been addressed by Niu et al. [14] through joint optimization of power allocation, transmit beamforming, and RIS phase shifts to maximize secrecy rates. Fascista et al. [15] offered a comprehensive solution for joint localization and synchronization in mmWave systems using optimized BS precoding and RIS phase profiles. Liu et al. [16] further advanced this field with a double active RIS-assisted radarcommunication coexistence system, employing penalty dual decomposition to solve the non-convex optimization problem of maximizing communication data rates. These studies

collectively demonstrate the trend toward multi-dimensional optimization in RIS-assisted systems, yet they predominantly focus on conventional performance metrics such as data rate and security, leaving energy efficiency considerations largely unexplored.

The integration of artificial intelligence (AI) next-generation communication systems, such as space-air-ground integrated networks envisioned for 6G, highlights the importance of AI-enabled resource optimization for ubiquitous connectivity [17]. Federated learning (FL) has emerged as a transformative distributed learning paradigm that effectively safeguards user privacy by keeping raw data locally stored while transmitting only gradient parameters. The FL research landscape has evolved along two primary dimensions: communication efficiency and model performance optimization. To address the communication bottleneck, Wu et al. [18] developed adaptive mutual knowledge distillation with dynamic gradient compression techniques, significantly reducing communication overhead. Zhang et al. [19] proposed adaptive parameter update rules that enhance test accuracy while minimizing communication costs. On the model performance front, Wu et al. [20] introduced cosine similarity-based weight coefficients for improved aggregation, while Chen et al. [21] designed a dynamic weighted averaging algorithm based on maximum mean discrepancy. Systemlevel innovations include asynchronous federated stochastic gradient descent algorithm [22], which demonstrates higher efficiency than synchronous approaches, and integration of FL with edge computing for distributed model updates [23]. Peng et al. [24] addressed noise interference challenges through the FedNoise algorithm with separate client-server learning rates. However, the aforementioned FL studies assume ideal communication channels, thereby neglecting the impact of physical wireless channel constraints. In particular, energy consumption poses a critical challenge for practical FL deployment, especially when battery-constrained IoT devices participate in distributed learning tasks.

To bridge the gap between algorithmic FL and physical layer realities, recent research has begun to integrate RIS into FL systems [25]. Foundational studies have shown that RIS can effectively mitigate communication errors during the FL process. Building on this, more advanced works have focused on joint resource allocation and beamforming design to directly enhance learning performance, for instance, by maximizing device participation under aggregation error constraints in over-the-air computation systems or by optimizing spectrum learning frameworks [26-27]. In a complementary direction, FL has also been leveraged as a tool to solve traditional wireless challenges, such as performing distributed channel estimation with reduced overhead [28-30]. Beside, Wang et al. [31] introduced a graph neural network (GNN)-based algorithm for scalable and efficient model aggregation for RISassisted over-the-air FL framework. Despite these significant contributions, the primary focus of existing work has been on improving learning accuracy or reducing communication latency. The critical issue of energy efficiency in these systems remains largely unexplored. This oversight represents a significant research gap, as a truly practical system must balance learning performance with sustainable energy consumption.

This paper investigates the critical yet under-explored problem of energy efficiency (EE) maximization in FL-assisted RIS-IoT networks. To address the highly non-convex and coupled nature of this problem, we propose an effective iterative optimization framework based on the synergy of successive convex approximation (SCA) and the alternating direction method of multipliers (ADMM). The main contributions are summarized as follows:

- We propose an FL-aware adaptive optimization strategy. By leveraging the gradient information inherent to the FL process, we design a dynamic stopping criterion for the resource allocation algorithm. This allows the optimization to terminate once a desired learning performance is achieved, significantly reducing unnecessary computational overhead for energy-constrained IoT devices compared to fixed-iteration approaches.
- To solve the challenging joint active and passive beamforming subproblem, we introduce an efficient ADMM-based decomposition algorithm. This algorithm effectively decouples the optimization of the BS's active beamforming and the RIS's computationally-complex unit-modulus phase shifts, enabling them to be solved iteratively with high efficiency.
- Through extensive simulations, we validate the effectiveness of our proposed framework. The results not only show significant improvements in both EE and sum rate over baseline schemes but also empirically demonstrate the robust convergence of our algorithm, providing a practical and efficient solution for deploying FL in future RIS-assisted IoT systems.

The remainder of this paper is organized as follows. Section II introduces the system model. The proposed algorithm is presented in Section III. Section IV offers numerical results to demonstrate the performance of the proposed algorithm. Finally, the paper comes to a conclusion in Section V.

II. SYSTEM MODEL

In essence, our system establishes an iterative cooptimization loop of that synergistically integrates RIS with FL through an alternating optimization strategy. Specifically, the RIS phase shift configuration directly influences the wireless channel conditions that affect FL model transmission quality, while the FL convergence performance provides critical feedback for subsequent RIS reconfiguration.

To contextualize this co-optimization, let us consider an illustrative application scenario: a smart factory for equipment fault prediction. In this large-scale smart factory, numerous IoT sensors are deployed across production lines to continuously monitor the operational status of machinery (e.g., vibration, temperature, current). These sensors collaboratively train a real-time equipment fault prediction model using federated learning. Factory environments, typically characterized by metallic structures, present significant challenges for wireless communication due to severe signal blockages and multi-path effects. RIS arrays are strategically positioned on walls and beams to create more stable and reliable communication links. This practical scenario highlights the necessity and benefits of our proposed FL-assisted RIS co-design.

3

In this Section, we introduce the FL and RIS model respectively, detailing their individual components and how they are integrated within our framework.

A. Federated Learning Process

The model training process of FL is illustrated in Fig. 1. During FL, the devices download the latest global gradient parameters from the server for local training. After training their local models, the devices send their local gradient parameters back to the server. The server aggregates the received local gradient parameters to update the global model [32]. The aim of FL is to minimize the loss function, that is,

$$F(\mathbf{w}) = \frac{1}{K} \sum_{k=1}^{K} f(\mathbf{w}; \mathbf{x}_k, \mathbf{y}_k), \tag{1}$$

where **w** is the vector of gradient parameter, K is the number of training samples, $(\mathbf{x}_k, \mathbf{y}_k)$ represents the k-th input vector and the output vector, $f(\mathbf{w}; \mathbf{x}_k, \mathbf{y}_k)$ is the loss function related to $\mathbf{x}_k, \mathbf{y}_k$.

According to gradient descent method, the global model is updated by

$$\mathbf{w}_{t+1} = \mathbf{w}_t - \zeta \sum_{i=1}^K \nabla f_i(\mathbf{w}_t), \tag{2}$$

where ζ represents the learning rate, which is used to control the step size in each iteration, and t represents the number of the current iteration.

In the aggregation phase of FL, the BS needs to aggregate the local model updates (or gradient information) received from each participating device. While the classic FedAvg algorithm employs simple arithmetic averaging, which assigns equal weights to all devices, it often overlooks the heterogeneous communication conditions and resource capabilities of diverse mobile devices. This lack of differentiation can impede model convergence and even affect learning performance in wireless FL scenarios.

Inspired by [33], we adopt a channel-aware weighted aggregation mechanism for the global model update to address these challenges. This approach is particularly critical in our RIS-assisted wireless system, where the dynamically reconfigurable channels significantly impact the reliability and efficiency of local model transmissions. By weighting local updates based on communication link quality, our method ensures that clients experiencing better channel conditions contribute more prominently and reliably to the global model, thereby implicitly enhancing overall FL performance and crucially, supporting the overarching energy efficiency maximization by aligning communication quality with learning contributions.

The quality of the channel can be measured by the l_2 norm of the channel matrix. Define the channel between the k-th device and the BS as $\mathbf{h}_k(\mathbf{\Phi})$. The larger the value of $\|\mathbf{h}_k(\mathbf{\Phi})\|_2$, the better the quality of the channel.

After calculating the l_2 norm of the channel matrix between all devices and the BS, the BS will assign different weight parameters to aggregate the gradient according to the channel quality, which can be expressed as:

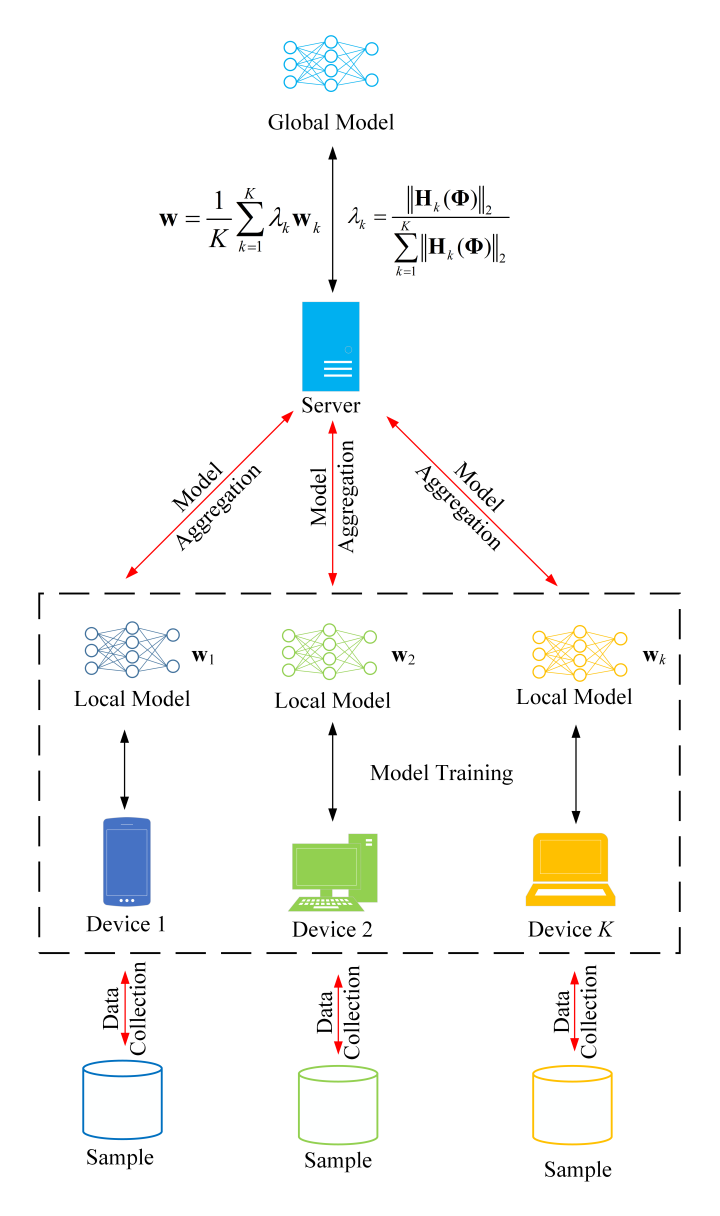


Fig. 1. FL process

$$\mathbf{w} = \frac{1}{K} \sum_{k=1}^{K} \lambda_k \mathbf{w}_k, \tag{3}$$

where λ_k is the weight parameter assigned to the k-th device, which can be calculated by

$$\lambda_k = \frac{\|\mathbf{h}_k(\mathbf{\Phi})\|_2}{\sum\limits_{k=1}^K \|\mathbf{h}_k(\mathbf{\Phi})\|_2}.$$
 (4)

It can be seen from the above formula that devices with better channel quality will get a larger weight coefficient, so that the gradient parameters of devices with good channel quality in the system occupy a larger proportion of the global model, accelerating the convergence speed of the global model. Crucially, the instantaneous channel quality, represented by the l_2 norm, is directly and dynamically influenced by the RIS passive beamforming and the BS active beamforming. This

Fig. 2. A RIS-assisted communication system model

establishes a fundamental feedback mechanism: the physical layer optimization, driven by RIS and BS beamforming, directly informs and enhances the FL aggregation process through these adaptive weights. This ensures that the FL algorithm is not oblivious to the underlying wireless conditions but actively leverages the improved communication environment to achieve more robust and efficient global model updates, thus enabling the "FL-assisted" component to be truly intelligent and responsive to the physical layer.

B. RIS-Assisted Communication Model

In this work, we consider a multi-user MISO downlink scenario where the BS utilizes spatial multiplexing to simultaneously transmit the global model parameters to K users within the same time-frequency resource block. The BS employs a dedicated beamforming vector $\boldsymbol{\theta}_k$ for each user k to focus the transmitted signal towards that user. Although the underlying informational content (the global model) is the same for all users, this concurrent spatial transmission inevitably creates inter-user interference, as the signal intended for user k acts as interference to other users. The objective of the beamforming design is precisely to manage this interference and maximize the desired signal power at each user.

The RIS-assisted communication model we use is shown in Fig. 2. The model includes a BS and K users and considers downlink data transmission. At this time, the transmission path includes the direct communication link from the BS to the device and the link reflected by the RIS. Define that the BS is configured with multiple antennas, the number of antennas is N, each device has a single antenna, and the number of RIS reflecting elements is L. Define the reflecting coefficient of the *l*-th RIS reflecting element is $\varphi_l = \tau_l e^{j\nu_l}, l = 1, 2, ..., L$, where $\tau_l \in (0,1]$ represents the reflection amplitude loss coefficient for element l, and $\nu_l \in (0, 2\pi]$ is the phase shift. In practical RIS implementations, due to imperfect materials and fabrication, τ_l is generally less than 1. For simplicity, we assume a uniform reflection amplitude loss across all elements, i.e., $\tau_l = \tau$ for all l. The reflection coefficient diagonal matrix of RIS is $\Phi = \operatorname{diag}(\tau e^{j\nu_1}, \tau e^{j\nu_2}, ..., \tau e^{j\nu_L}),$ where $diag(\cdot)$ represents the diagonal matrix. In addition, the signal transmitted by the BS is defined as \mathbf{x} , and beamforming

technology is used to support the transmission of data to the device. Therefore, the received signal of the k-th device can be expressed as:

$$\mathbf{y}_k = (\mathbf{h}_{BD,k} + \mathbf{h}_{BR} \mathbf{\Phi} \mathbf{h}_{RD,k}) \mathbf{x} + \mathbf{n}_k, \tag{5}$$

where $\mathbf{h}_{BD,k}$, \mathbf{h}_{BR} , $\mathbf{h}_{RD,k}$ represent the channel matrix from BS to the k-th device, from BS to RIS, from RIS to the k-th device, respectively. $\mathbf{n}_k \sim CN(0,\sigma_k^2)$ represents the additive white Gaussian noise. The composite channel vector $\mathbf{h}_k(\Phi) = \mathbf{h}_{\mathrm{BD},k} + \mathbf{h}_{\mathrm{BR}}\Phi\mathbf{h}_{\mathrm{RD},k}$ is crucial as it explicitly demonstrates the direct and tunable influence of the RIS phase shift matrix on the received signal at device k. This highlights how RIS actively reconfigures the wireless propagation environment, which in turn underpins the channel quality metric used for FL aggregation as discussed in Section II-A.

In practical communications, beamforming is first applied to make the energy of transmitted signal more concentrated. Assuming that the original signal component transmitted by the system to the device is s_j , the BS can design the transmission signal \mathbf{x} according to the following formula:

$$\mathbf{x} = \sum_{j=1}^{K} \boldsymbol{\theta}_{j} s_{j},\tag{6}$$

where θ_j is the bramforming vector of the BS. Therefore, the received signal of the k-th device can be written as:

$$\mathbf{y}_k = \mathbf{h}_k(\mathbf{\Phi}) \sum_{j=1}^K \boldsymbol{\theta}_j s_j + \mathbf{n}_k. \tag{7}$$

The above formula can be further divided into three parts of expected signal, interference signal, and noise:

$$\mathbf{y}_k = \mathbf{h}_k(\mathbf{\Phi})\boldsymbol{\theta}_k s_k + \mathbf{h}_k(\mathbf{\Phi}) \sum_{j=1, j \neq k}^K \boldsymbol{\theta}_j s_j + \mathbf{n}_k, \quad (8)$$

where the first item is the expected signal of the k-th device, the second item is the interference signal from the other devices, and the third item is the noise. Therefore, the signal to interference plus noise ratio (SINR) of the k-th device can be written as:

According to Shannon formula, the sum rate of all the devices can be written as:

$$R_{\text{sum}} = \sum_{k=1}^{K} \log_2 (1 + \gamma_k)$$
 (10)

In the design of modern wireless communication systems, particularly for the IoT, system sum rate is the most critical performance metrics. System sum rate, which represents the total data throughput for all users, is a direct measure of the system's capacity and its ability to provide a high quality of service. Maximizing the sum rate is essential for supporting the massive connectivity and high-data demands of emerging IoT applications. To improve the service quality between users and transmitters as much as possible, it is necessary to maximize the device's achievable communication rate under the condition of meeting the transmission power budget, forming the following optimization problem:

$$\max_{\mathbf{\Phi}, \theta} R_{\text{sum}} = \sum_{k=1}^{K} \log_2 \left(1 + \gamma_k \right). \tag{11}$$

Simultaneously, energy efficiency, defined as the ratio of the sum rate to total power consumption, has become a paramount concern. This is motivated by two key factors. Firstly, many IoT devices are battery-powered, and high energy efficiency is crucial for extending their operational lifetime and reducing maintenance costs. Meanwhile, from the network perspective, reducing the power consumption of network infrastructure, such as base stations, lowers operational expenditures and contributes to environmentally sustainable or green communications, a key goal for 6G networks. In order to analyze the energy efficiency of the system, it is necessary to analyze the power consumption of the system. The total power consumption of the system consists of the transmission power of the BS and the power consumed by each component, and can be expressed as:

$$P_{\text{total}} = \xi \|\boldsymbol{\theta}\|^2 + P_B + K \cdot P_D + N \cdot P_R \tag{12}$$

where ξ is the inverse of the transmit power amplifier efficiency, P_B , P_D , P_R are the power consumption of the BS, a device and a RIS reflecting element. Therefore, the energy efficiency can be defined as:

$$\eta_{EE} = \frac{R_{\text{sum}}}{P_{\text{total}}}.$$
 (13)

The energy efficiency problem of the system can be expressed as:

$$\max_{\theta, \Phi} \eta_{EE} = \frac{\sum_{k=1}^{K} \log_2 (1 + \gamma_k)}{\xi \|\theta\|^2 + P_B + K \cdot P_D + N \cdot P_R}$$
(14)

s.t.
$$\sum_{k=1}^{K} \|\theta_k\|^2 \le P_{\text{max}}$$
 (15)

5

$$|\varphi_l| = \tau, l = 1, 2, ..., Lx$$
 (16)

where the first constraint limits the maximum transmission power of the BS to $P_{\rm max}$, and the second constraint constrains the RIS reflection coefficient with a constant modulus condition. It can be seen that the above energy efficiency optimization problem is a non-convex optimization problem. In the next Section, we will use the proposed algorithm to optimize this problem.

III. ACTIVE AND PASSIVE BEAMFORMING BASED ON SCA AND ADMM ALGORITHMS

A. Optimization of FL Iteration Using SCA Algorithm

The basic process of the SCA algorithm is to approximate each non-convex part of a non-convex problem as a convex function at a certain point, and then solve the approximated convex problem. The SCA algorithm operates iteratively. In each iteration, it constructs a tractable convex approximation of the original non-convex problem, localized around the solution obtained from the previous iteration. This approximated problem is then solved to generate the next iterate. This process is repeated, generating a sequence of solutions that are guaranteed to converge to a stationary point of the original problem, which corresponds to a locally optimal or suboptimal solution. In Section II, the loss function of FL is non-convex, therefore we introduce a quadratic approximation convex surrogate function:

$$g(\mathbf{w}, \mathbf{w}_t) = f(\mathbf{w}_t) + \langle \nabla f(\mathbf{w}_t), \mathbf{w} - \mathbf{w}_t \rangle + \frac{1}{2} (\mathbf{w} - \mathbf{w}_t)^{\mathrm{T}} \mathbf{H}_t (\mathbf{w} - \mathbf{w}_t),$$
(17)

where $\nabla f(\mathbf{w}_t)$ is the gradient vector at \mathbf{w}_t , \mathbf{H}_t is the Hessian matrix at \mathbf{w}_t . Therefore, the update formula of the global model parameters can be expressed as:

$$\mathbf{w}_{t+1} = \mathbf{w}_t - \zeta \sum_{i=1}^K \nabla g_i(\mathbf{w}_t). \tag{18}$$

After each iteration, the average value of the gradients uploaded by all devices is calculated by

$$\overline{\nabla}(\mathbf{w}_{t+1}) = \frac{1}{K} \sum_{i=1}^{K} \nabla g_i(\mathbf{w}_{t+1}). \tag{19}$$

The stopping criterion of the iteration is related to the average gradient. We set the threshold ϵ , when $\left\|\overline{\nabla}(\mathbf{w}_{t+1})\right\|_2 < \varepsilon$, the iteration stops. In this paper, we set the convergence threshold $\varepsilon = 10^{-4}$. The selection of this specific threshold is based on a trade-off between achieving sufficient optimization

accuracy and computational efficiency. A smaller ε would lead to a more precise convergence point, potentially yielding a marginally higher energy efficiency. However, it would also require a greater number of iterations, thereby increasing the computational time. Conversely, a larger ε would result in faster convergence but might terminate prematurely, leading to a suboptimal solution.

B. Transformation of Energy Efficiency Optimization Problem

To address the complex form of the objective function in energy efficiency optimization problems, the objective function can be decoupled using the method of Lagrangian dual reconstruction. Introducing the auxiliary variable $\alpha = [\alpha_1, \alpha_1, ..., \alpha_K]^T$, the original problem can be equivalently transformed into the following form:

$$\max_{\boldsymbol{\theta}, \boldsymbol{\Phi}, \boldsymbol{\alpha}} \sum_{k=1}^{K} \left[(1 + \alpha_k) \frac{\left| \mathbf{h}_k^{H}(\boldsymbol{\Phi}) \boldsymbol{\theta}_k \right|^2}{\sum_{j=1}^{K} \left| \mathbf{h}_k^{H}(\boldsymbol{\Phi}) \boldsymbol{\theta}_j \right|^2 + \sigma_k^2} + \log_2 (1 + \alpha_k) - \alpha_k \right] - \eta_{EE} P_{\text{total}},$$
 (20)

s.t.
$$\sum_{k=1}^{K} \|\boldsymbol{\theta}_k\|^2 \le P_{\text{max}},$$
 (21)

$$|\varphi_l| = \tau, \quad l = 1, 2, \dots, L. \tag{22}$$

Introducing the auxiliary variable $\beta = [\beta_1, \beta_2, ..., \beta_K]^T$, and using the quadratic transformation, the above problem is converted into the following form:

$$\max_{\boldsymbol{\theta}, \boldsymbol{\Phi}, \boldsymbol{\alpha}, \boldsymbol{\beta}} f_1(\boldsymbol{\theta}, \boldsymbol{\Phi}, \boldsymbol{\alpha}, \boldsymbol{\beta}), \tag{23}$$

s.t.
$$\sum_{k=1}^{K} \|\boldsymbol{\theta}_k\|^2 \le P_{\max},$$
 (24)

$$|\varphi_l| = \tau, l = 1, 2, ..., L,$$
 (25)

where the object function $f_1(\boldsymbol{\theta}, \boldsymbol{\Phi}, \boldsymbol{\alpha}, \boldsymbol{\beta})$ is

$$\sum_{k=1}^{K} \left[-|\beta_{k}|^{2} \left(\sum_{j=1}^{K} \left| \mathbf{h}_{k}^{H}(\mathbf{\Phi}) \boldsymbol{\theta}_{j} \right|^{2} + \sigma_{k}^{2} \right) + \log_{2} \left(1 + \alpha_{k} \right) \right.$$
$$\left. - \alpha_{k} + 2\sqrt{1 + \alpha_{k}} \operatorname{Re} \left\{ \beta_{k} \mathbf{h}_{k}^{H}(\mathbf{\Phi}) \boldsymbol{\theta}_{k} \right\} \right] - \eta_{EE} P_{\text{total}}. \tag{26}$$

The alternating optimization method can be used to perform cyclic optimization updates on the four variables. By taking partial derivatives of the auxiliary variables α and β in $f_1(\theta, \Phi, \alpha, \beta)$ and setting them equal to zero, we can obtain the optimal solutions α^{opt} and β^{opt} for the auxiliary variables α and β , respectively, that is,

$$\frac{\partial f_1}{\partial \alpha_k} = 0, \frac{\partial f_1}{\partial \beta_k} = 0, k = 1, 2, ..., K. \tag{27}$$

At this point, the components of the auxiliary variables α and β can be obtained as follows:

$$\alpha_k^{\text{opt}} = \frac{c_k(c_k + \sqrt{c_k^2 + 4})}{2},$$
(28)

$$\beta_k^{\text{opt}} = \frac{\sqrt{1 + \alpha_k} \mathbf{h}_k^{\text{H}}(\mathbf{\Phi}) \boldsymbol{\theta}_k}{\sum_{k=1}^K \left| \mathbf{h}_k^{\text{H}}(\mathbf{\Phi}) \boldsymbol{\theta}_j \right|^2 + \sigma_k^2},$$
 (29)

where $c_k = \text{Re}\{\beta_k \mathbf{h}_k^{\text{H}}(\mathbf{\Phi})\boldsymbol{\theta}_k\}.$

C. Solution of Active Beamforming Vector at BS

When auxiliary variables α , β , and passive beamforming vector Φ at RIS is fixed, we can solve the optimized solution θ^{opt} of the active beamforming vector θ at BS. To simplify the objective function, we have the following definitions:

$$\mathbf{A} \triangleq \mathbf{I}_k \otimes \left(\eta_{EE} \xi \mathbf{I}_k + \sum_{k=1}^K |\beta_k|^2 \mathbf{h}_k(\mathbf{\Phi}) \mathbf{h}_k^{\mathrm{H}}(\mathbf{\Phi}) \right), \quad (30)$$

$$\mathbf{v}_k \triangleq \sqrt{1 + \alpha_k} \beta_k \mathbf{h}_k(\mathbf{\Phi}), \tag{31}$$

$$\mathbf{V} \triangleq \begin{bmatrix} \mathbf{v}_1^{\mathrm{H}}, \mathbf{v}_2^{\mathrm{H}}, ..., \mathbf{v}_K^{\mathrm{H}} \end{bmatrix}^{\mathrm{H}}.$$
 (32)

Therefore, the object function can be written as:

$$f_1(\boldsymbol{\theta}) = -\boldsymbol{\theta}^{\mathrm{H}} \boldsymbol{A} \boldsymbol{\theta} + 2 \operatorname{Re} \left[\mathbf{V}^{\mathrm{H}} \boldsymbol{\theta} \right].$$
 (33)

The optimization problem can be written as:

$$\min_{\boldsymbol{\theta}} f_2(\boldsymbol{\theta}) = \boldsymbol{\theta}^{\mathsf{H}} \boldsymbol{A} \boldsymbol{\theta} - 2 \operatorname{Re} \left[\mathbf{V}^{\mathsf{H}} \boldsymbol{\theta} \right], \tag{34}$$

s.t.
$$\theta^{\mathrm{H}} D\theta \le P_{\mathrm{max}},$$
 (35)

where $D = I_K \otimes I_N$. The above optimization problem is a quadratic constrained quadratic programming problem, and the optimal solution can be obtained using the ADMM algorithm.

The feasible region $\mathcal G$ of the constraint function is defined as:

$$I_{\mathcal{G}}(\mathbf{Q}) \triangleq \begin{cases} 0, & \mathbf{Q} \in \mathcal{G}, \\ +\infty, & \text{otherwise,} \end{cases}$$
 (36)

where auxiliary variable $\mathbf{Q} = \boldsymbol{\theta}$. Therefore, the problem is equivalent to

$$\min_{\boldsymbol{\theta}, \mathbf{Q}} \mathbf{Q}^H \mathbf{A} \mathbf{Q} - 2 \operatorname{Re} \left[\mathbf{V}^H \mathbf{Q} \right] + I_{\mathcal{G}}(\mathbf{Q}), \tag{37}$$

s.t.
$$\mathbf{Q} = \boldsymbol{\theta}$$
. (38)

Construct the augmented Lagrangian function:

$$\mathcal{L}_{\rho}(\mathbf{Q}, \boldsymbol{\theta}, \boldsymbol{\omega}) = \mathbf{Q}^{H} \mathbf{A} \mathbf{Q} - 2 \operatorname{Re} \left[\mathbf{V}^{H} \mathbf{Q} \right] - \operatorname{Re} \left[\boldsymbol{\omega} (\mathbf{Q} - \boldsymbol{\theta}) \right] + \frac{\rho}{2} \| \mathbf{Q} - \boldsymbol{\theta} \|_{2}^{2}$$
(39)

where $\rho > 0$ is the penalty term, ω is the Lagrange dual variable. Alternately optimize variables \mathbf{Q} , $\boldsymbol{\theta}$, and $\boldsymbol{\omega}$:

$$\mathbf{Q}^{t+1} = \arg\min_{\mathbf{Q}} \mathcal{L}_{\rho}(\mathbf{Q}^{t}, \boldsymbol{\theta}^{t}, \boldsymbol{\omega}^{t}), \tag{40}$$

$$\boldsymbol{\theta}^{t+1} = \arg\min_{\boldsymbol{\theta}} \mathcal{L}_{\rho}(\mathbf{Q}^{t+1}, \boldsymbol{\theta}^{t}, \boldsymbol{\omega}^{t}), \tag{41}$$

$$\boldsymbol{\omega}^{t+1} = \boldsymbol{\omega}^t - \rho(\mathbf{Q}^{t+1} - \boldsymbol{\theta}^{t+1}). \tag{42}$$

Since the above Lagrangian function is convex, the closed-form solution of θ can be obtained according to the first-order optimal condition. By taking the partial derivative of the Lagrangian function with respect to \mathbf{Q} , we have:

$$\frac{\partial \mathcal{L}_{\rho}}{\partial \mathbf{Q}} = 2\mathbf{A}\mathbf{Q}^{t+1} - 2\mathbf{V} - \boldsymbol{\omega}^{t} + \rho(\mathbf{Q}^{t+1} - \boldsymbol{\theta}^{t}). \tag{43}$$

Setting the partial derivative equal to 0, we have:

$$\mathbf{Q}^{t+1} = (2\mathbf{A} + \rho \mathbf{I}_K)^{-1} (2\mathbf{V} + \boldsymbol{\omega}^t + \rho \boldsymbol{\theta}^t). \tag{44}$$

Then we can optimize θ . By taking the partial derivative of of the Lagrangian function with respect to θ , we have:

$$\frac{\partial \mathcal{L}_{\rho}}{\partial \boldsymbol{\theta}} = \boldsymbol{\omega}^{t} - \rho (\mathbf{Q}^{t+1} - \boldsymbol{\theta}^{t+1}). \tag{45}$$

Setting the partial derivative equal to 0, we have:

$$\boldsymbol{\theta}^{t+1} = \mathbf{Q}^{t+1} - \rho^{-1} \boldsymbol{\omega}^t, \tag{46}$$

$$\boldsymbol{\omega}^{t+1} = 2\mathbf{A}\mathbf{Q}^{t+1} - 2\mathbf{V}.\tag{47}$$

The update of θ iteratively refines the BS transmit beamforming, directly influencing the downlink channel quality and thus the data rates to the devices. Its convergence reflects the optimization of power allocation and directional transmission to maximize the objective function given the current RIS configuration and local device accuracies.

D. Solution of Passive Beamforming Vector at RIS

When auxiliary variables α , β , and active beamforming vector θ at BS is fixed, we can solve the optimized solution of the passive beamforming vector at RIS. The optimization problem $\max_{\Phi} f_3(\Phi)$ can be written as:

$$\sum_{k=1}^{K} \left[\log_2(1 + \alpha_k) - \alpha_k + 2\sqrt{1 + \alpha_k} \operatorname{Re} \left\{ \beta_k \mathbf{h}_k^{\mathrm{H}} \boldsymbol{\theta}_k \right\} - |\beta_k|^2 \left(\sum_{j=1}^{K} \left| \mathbf{h}_k^{\mathrm{H}} \boldsymbol{\theta}_j \right|^2 + \sigma_k^2 \right) \right] - \eta_{EE} P_{\max}.$$
 (48)

Similar to the optimization process of the active beamforming vector at BS, the optimization problem can be rewritten as:

$$\mathbf{\Phi} = \operatorname*{arg\,min}_{\mathbf{\Phi}} f_4(\mathbf{\Phi}) = \mathbf{\Phi}^{\mathsf{H}} \mathbf{B} \mathbf{\Phi} - 2 \operatorname{Re} \left[\mathbf{\Phi}^{\mathsf{H}} \mathbf{u} \right], \tag{49}$$

s.t.
$$|\varphi_l| = \tau, l = 1, 2, ..., L,$$
 (50)

where matrix B and u are:

$$\mathbf{B} = \sum_{k=1}^{K} |\beta_k|^2 \sum_{j=1}^{K} \mathbf{h}_k^{\mathrm{H}}(\mathbf{\Phi}) \boldsymbol{\theta}_j \boldsymbol{\theta}_j^{\mathrm{H}} \mathbf{h}_k(\mathbf{\Phi}), \tag{51}$$

$$\mathbf{u} = \sum_{k=1}^{K} \sqrt{(1 + \alpha_k)} \beta_k \mathbf{h}_k^{\mathrm{H}}(\mathbf{\Phi}) \boldsymbol{\theta}_k.$$
 (52)

The object function is convex, while the constraint is non-convex. Relaxing it to the convex constraint condition of $|\varphi_l| \leq 1$ can transform the optimization problem into a quadratic constrained quadratic programming problem, and the ADMM algorithm can be used to obtain the sub-optimal solution.

The feasible region ${\cal H}$ of the constraint function is defined as:

$$I_{\mathcal{H}}(\mathbf{q}) \triangleq \begin{cases} 0, & \mathbf{q} \in \mathcal{H}, \\ +\infty, & \text{otherwise,} \end{cases}$$
 (53)

where auxiliary variable $\mathbf{q} = \mathbf{\Phi}$. Therefore, the optimization problem is equal to

$$\min_{\mathbf{\Phi}, \mathbf{q}} \mathbf{q}^{\mathsf{H}} \mathbf{B} \mathbf{q} - 2 \operatorname{Re} \left[\mathbf{q}^{\mathsf{H}} \mathbf{u} \right] + I_{\mathcal{H}}(\mathbf{q}), \tag{54}$$

s.t.
$$\mathbf{q} = \mathbf{\Phi}$$
. (55)

Construct the augmented Lagrangian function:

$$\mathcal{L}_{\delta}(\mathbf{q}, \mathbf{\Phi}, \boldsymbol{\mu}) = \mathbf{q}^{\mathsf{H}} \mathbf{B} \mathbf{q} - 2 \operatorname{Re} \left[\mathbf{q}^{\mathsf{H}} \mathbf{u} \right] - \operatorname{Re} \left[\boldsymbol{\mu} (\mathbf{q} - \mathbf{\Phi}) \right] + \frac{\delta}{2} \|\mathbf{q} - \mathbf{\Phi}\|_{2}^{2}$$
(56)

where $\delta > 0$ is the penalty term, μ is the Lagrange dual variable. Alternately optimize variables \mathbf{q} , Φ , and μ :

$$\mathbf{q}^{t+1} = \operatorname*{arg\,min}_{\mathbf{q}} \mathcal{L}_{\delta}(\mathbf{q}^t, \mathbf{\Phi}^t, \boldsymbol{\mu}^t), \tag{57}$$

$$\mathbf{\Phi}^{t+1} = \arg\min_{\mathbf{\Phi}} \mathcal{L}_{\delta}(\mathbf{q}^{t+1}, \mathbf{\Phi}^{t}, \boldsymbol{\mu}^{t}), \tag{58}$$

$$\mathbf{\Phi}^{t+1} = \arg\min_{\mathbf{\Phi}} \mathcal{L}_{\delta}(\mathbf{q}^{t+1}, \mathbf{\Phi}^{t}, \boldsymbol{\mu}^{t}). \tag{59}$$

Since the above Lagrangian function is convex, the closed-form solution of Φ can be obtained according to the first-order optimal condition. By taking the partial derivative of the Lagrangian function with respect to \mathbf{q} , we have:

$$\frac{\partial \mathcal{L}_{\delta}}{\partial \mathbf{q}} = 2\mathbf{B}\mathbf{q}^{t+1} - 2\mathbf{u} - \boldsymbol{\mu}^{t} + \delta(\mathbf{q}^{t+1} - \boldsymbol{\Phi}^{t}). \tag{60}$$

Setting the partial derivative equal to 0, we have:

$$\mathbf{q}^{t+1} = (2\mathbf{B} + \delta \mathbf{I}_N)^{-1} (2\mathbf{u} + \boldsymbol{\mu}^t + \delta \boldsymbol{\Phi}^t). \tag{61}$$

Then we can optimize Φ . By taking the partial derivative of of the Lagrangian function with respect to Φ , we have:

$$\frac{\partial \mathcal{L}_{\delta}}{\partial \mathbf{\Phi}} = \boldsymbol{\mu}^{t} - \delta(\mathbf{q}^{t+1} - \mathbf{\Phi}^{t+1}). \tag{62}$$

Setting the partial derivative equal to 0 and considering the constraint, we have:

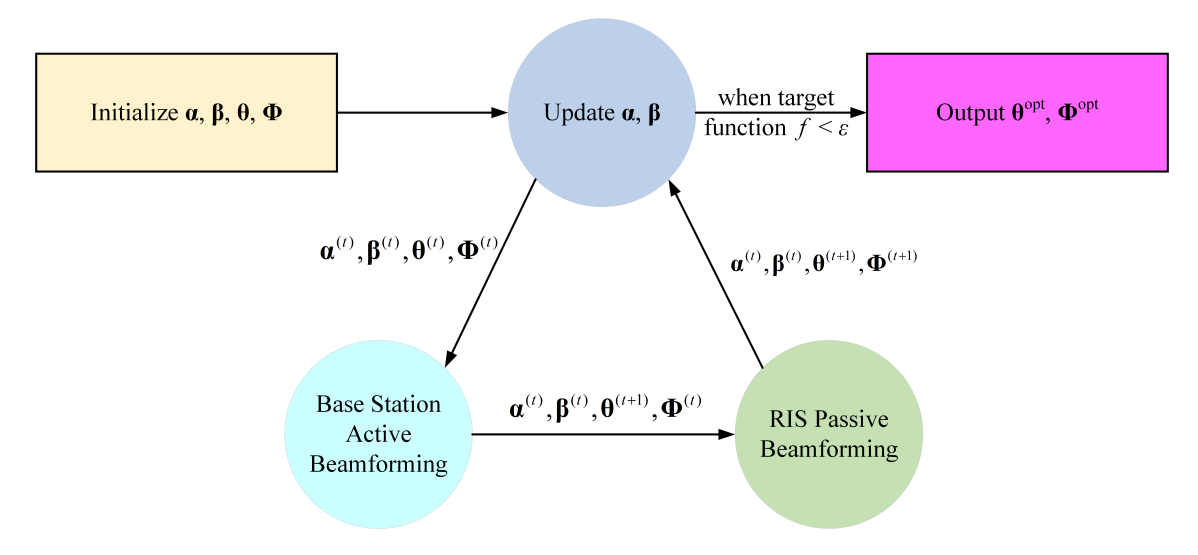


Fig. 3. Iterative update process of each variable of ADMM algorithm

$$\mathbf{\Phi}^{t+1} = \frac{\mathbf{q}^{t+1} - \delta^{-1} \boldsymbol{\mu}^t}{|\mathbf{q}^{t+1} - \delta^{-1} \boldsymbol{\mu}^t|}.$$
 (63)

Finally, we can optimize the Lagrange dual variable μ and obtain its expression:

$$\boldsymbol{\mu}^{t+1} = 2\mathbf{B}\mathbf{q}^{t+1} - 2\mathbf{u}.\tag{64}$$

The update of Φ dynamically adjusts the RIS reflection coefficients. This step is crucial for constructively combining signals to enhance desired paths and mitigate interference. Its convergence signifies that the optimal passive beamforming pattern for the current active beamforming and device requirements has been achieved, maximizing the RIS's collaborative gain.

Our proposed iterative optimization framework intrinsically couples the RIS-assisted beamforming design with the FL training and aggregation process to maximize system energy efficiency. Each iteration represents a cycle where communication resources are optimized to explicitly facilitate FL, and FL's aggregation strategy intelligently utilizes the resulting communication conditions. Specifically, the framework involves alternating updates between the FL-aware communication parameters and auxiliary variables that mediate the FL performance within the energy efficiency objective. The channel information, dynamically shaped by RIS and active beamforming, directly influences parameters like the FL aggregation weights and the auxiliary variables for the EE problem, thus establishing a closed-loop co-design. The general analysis of the convergence of ADMM can be found in [34].

The optimization iterative process of each variable is summarized in Algorithm 1, and its flow chart is shown in Fig. 3. This algorithm takes maximizing the system energy efficiency as the optimization goal, and iterates the four variables alternately until the objective function converges. Crucially, in each iteration, the updated RIS phase shifts and active beamforming vectors directly impact the communication channels. This refreshed channel information then feeds into the calculation of Algorithm 1 Iterative update process of each variable of ADMM algorithm

Input: Channel matrix $\mathbf{H}_k(\mathbf{\Phi}), k = 1, 2, ..., K$, threshold ε , maximum transmission power of BS P_{max}

1 Initialization: $\Phi^{(0)}, \theta^{(0)}, \alpha^{(0)}, \beta^{(0)}$

2 Set t = 1

3 repeat

Replace auxiliary variable $\alpha^{(t)}$ by (28) 4

Calculate intermediate variable $\beta^{(t)}$ via (29) 5

Update active beamforming vector $\boldsymbol{\theta}^{(t)}$ at BS following 6 $\boldsymbol{\theta}^{(t)} = \mathbf{Q}^{(t)} - \rho^{-1} \boldsymbol{\omega}^{(t-1)}$

Renew passive beamforming vector $\mathbf{\Phi}^{(t)}$ at RIS according to $\mathbf{\Phi}^{(t)} = \frac{\mathbf{q}^{(t)} - \delta^{-1} \boldsymbol{\mu}^{(t-1)}}{\left|\mathbf{q}^{(t)} - \delta^{-1} \boldsymbol{\mu}^{(t-1)}\right|}$ Compute the sum rate R_{sum} as mentioned in 7

8

$$R_{\mathrm{sum}} = \sum_{k=1}^{K} \log_2{(1+\gamma_k)}$$
 Determine the energy efficiency η_{EE} based on

9

$$\eta_{EE} = rac{R_{
m sum}}{P_{
m total}} \ t = t+1$$

10

11 until $f = R_{\text{sum}} - \eta_{EE} P_{\text{max}} < \varepsilon$ 12 return $\Phi^{(\text{opt})}, \theta^{(\text{opt})}, R_{\text{sum}}, \eta_{EE}$

the FL aggregation weights, ensuring a dynamic and channelaware FL process. This iterative dependency highlights the tight coupling between the communication layer optimization and the FL training process, where RIS's role is to enable efficient communication for FL, and FL's role is to leverage those efficiencies for better learning outcomes and overall system EE.

The total computational complexity per ADMM iteration is dominated by the most intensive subproblem. In our case, it is primarily driven by the active beamforming optimization and passive beamforming optimization. Therefore, the overall complexity per iteration is approximately $O(N^3K^3 + L^3)$. For typical large-scale IoT systems, the number of devices Kcan be very large, while the number of BS antennas N and RIS elements L are usually of moderate size. Our algorithm's

complexity per iteration grows polynomially with K, N, and L. For massive MIMO arrays, very large RIS arrays, or a large number of IoT devices, the terms could become significant.

To provide a comprehensive comparison with classical optimization techniques, we consider a direct gradient descent (GD) approach applied to our non-convex energy efficiency maximization problem. A single iteration of GD would involve calculating the gradients of the objective function with respect to all optimization variables. This typically requires operations such as computing composite channel vectors, SINRs, and power consumption terms. Specifically, evaluating the gradient with respect to $\boldsymbol{\theta}$ and $\boldsymbol{\Phi}$ would involve numerous matrix-vector multiplications and element-wise operations. While a detailed derivation of GD's complexity for this specific nonconvex problem is intricate, it is generally on the order of $O\left(KN^2+KL^2\right)$, and crucially, it typically avoids the computationally expensive matrix inversion operations present in our ADMM subproblems.

Comparing these, a single iteration of a basic gradient descent method might appear computationally less intensive than one iteration of our SCA-ADMM algorithm due to the lack of matrix inversions. However, for highly non-convex and coupled problems like ours, direct gradient descent methods are known to suffer from slow convergence or even fail to converge to high-quality solutions. They are highly sensitive to learning rate selection and prone to getting stuck in poor local optima. In contrast, our SCA-ADMM approach, by iteratively solving convex approximations via ADMM, leverages stronger theoretical guarantees for converging to a stationary point of the original non-convex problem. This robust convergence property, coupled with potentially fewer overall iterations needed to achieve a satisfactory solution quality, often makes the SCA-ADMM algorithm more efficient in practice, despite its higher per-iteration complexity. Therefore, further research on low-complexity approximation methods would be necessary.

IV. SIMULATION RESULTS

A. Simulation Settings

To accurately reflect the signal transmission characteristics in the real environment, the channel used in the simulation is the Ricean channel, which is consistent with the two paths in the communication model: from the BS to the device directly and from the BS to the device via the RIS array. The SNR for the simulation is set at 20 dB. This value is selected to represent a moderate to good signal quality environment, allowing the observation of beamforming gains while also reflecting realistic conditions where noise and interference are present. It is a common benchmark in wireless communication studies to evaluate system performance effectively under favorable yet practical conditions.

The BS is equipped with 4 antennas. This configuration represents a common multi-antenna BS setup, suitable for spatial multiplexing and beamforming in current and near-future IoT deployments, balancing complexity and performance gains. The power consumption per RIS reflecting element is set to 0 dBm. This value reflects the generally very low power

consumption of passive RIS elements, primarily for control circuitry, which is a key advantage of RIS technology for energy efficiency and aligns with typical assumptions in RIS power models. The power consumption per user device is chosen as 10 dBm. This represents a typical power consumption for an IoT device undergoing active communication and local computation, balancing the energy cost of data transmission and local model processing in a realistic scenario. The learning rate for FL is set to 0.05. This value is empirically chosen within the commonly accepted range for federated learning algorithms to balance convergence speed and solution stability. It ensures that the model updates are significant enough to progress efficiently without causing oscillations. The total number of users is set to 40. This number reflects a moderately dense IoT environment, typical for applications like smart cities or industrial IoT, where a significant but manageable number of devices participate in the FL process, allowing us to evaluate the system's performance under practical multiuser conditions.

The coordinates of the BS at (0, -50 m, 3 m), the RIS at (20 m, 10 m, 5 m), and the center coordinates of the devices at (40 m, 0, 0) are chosen to represent a typical urban or suburban IoT deployment scenario. This configuration allows for both a direct line-of-sight path and an RIS-assisted path, reflecting realistic signal propagation environments where RIS can effectively mitigate blockages or enhance received signal strength. The specific distances are set to explore performance in a moderately sized service area, consistent with common cellular communication ranges for IoT devices. The number of reflective elements in the RIS array, the number of iterations in FL, the transmission power of the BS, and the reflection amplitude loss of the RIS elements are the variables in the simulation.

TABLE I SIMULATION PARAMETERS

| Parameters | Values | | |
|------------------------------|----------------|--|--|
| Coordinate of BS | (0, -50m, 3m) | | |
| Coordinate of RIS | (20m, 10m, 5m) | | |
| Center coordinate of devices | (40m, 0, 0) | | |
| Learning rate | 0.05 | | |
| Number of devices | 40 | | |
| Number of BS antennas | 4 | | |
| RIS power consumption | 0 dBm | | |
| Device power consumption | 10 dBm | | |

For the FL model, we employ a convolutional neural network (CNN) architecture comprising two 5×5 convolutional layers, each followed by 2×2 max pooling, a normalization layer, a fully connected layer, a ReLU activation, and a Softmax output. The cross-entropy function serves as the loss function. This CNN architecture is a standard and widely adopted benchmark model for FL research, particularly suitable for resource-constrained IoT devices due to its moderate complexity, enabling fair comparison with existing FL literature. We use the sum rate and energy efficiency as evaluation

TABLE II
SIMULATION RESULTS (MEAN±STD) OF THE PROPOSED SCA-ADMM ALGORITHM AND COMPARISON METHODS UNDER DIFFERENT SYSTEM SETTINGS.

| Scenario | SCA-ADMM | SCA | P-BF [6] / RCG [11] / FedAvg | Random Phase Shift | w/o FL | w/o RIS | | |
|---------------------------------|--|------------------|------------------------------|--------------------|--------------------|------------------|--|--|
| Sum Rate vs. RIS Elements | | | | | | | | |
| 8 | 22.36 ± 0.41 | 18.31 ± 0.51 | 20.20±0.48 (P-BF) | 16.14 ± 0.62 | 14.35 ± 0.78 | - | | |
| 16 | 29.08 ± 0.44 | 25.89 ± 0.45 | 27.15±0.49 (P-BF) | 21.95 ± 0.54 | $20.82 {\pm} 0.65$ | - | | |
| 32 | $39.84 {\pm} 0.40$ | 36.32 ± 0.46 | 38.10±0.45 (P-BF) | 31.14 ± 0.50 | 30.36 ± 0.56 | - | | |
| 64 | 48.24 ± 0.38 | 45.31 ± 0.43 | 47.35±0.47 (P-BF) | 41.18 ± 0.49 | 40.34 ± 0.58 | - | | |
| Sum Rate vs. Transmit Power (W) | | | | | | | | |
| 0.2 | $29.89 {\pm} 0.20$ | 23.46 ± 0.23 | 25.78±0.20 (RCG) | 22.07 ± 0.25 | 13.96 ± 0.38 | 6.85 ± 0.42 | | |
| 0.5 | 34.30 ± 0.23 | 27.27 ± 0.28 | 30.29±0.22 (RCG) | 25.09 ± 0.31 | 16.97 ± 0.43 | 9.86 ± 0.51 | | |
| 0.8 | 41.54 ± 0.25 | 31.64 ± 0.32 | 37.43±0.26 (RCG) | 27.32 ± 0.34 | 19.21 ± 0.46 | 12.10 ± 0.56 | | |
| 1.0 | 47.80 ± 0.27 | 35.46 ± 0.35 | 43.79±0.28 (RCG) | 28.28 ± 0.35 | 20.17 ± 0.51 | 13.06 ± 0.60 | | |
| | Energy Efficiency vs. Transmit Power (W) | | | | | | | |
| 0.2 | 1.19 ± 0.05 | 1.12 ± 0.08 | 1.17±0.05 (RCG) | 1.07 ± 0.10 | 1.12 ± 0.11 | 0.92 ± 0.09 | | |
| 0.8 | 1.79 ± 0.07 | 1.70 ± 0.09 | 1.77±0.08 (RCG) | 1.57 ± 0.13 | 1.62 ± 0.10 | 1.42 ± 0.12 | | |
| 1.2 | 2.02 ± 0.09 | 1.94 ± 0.11 | 2.00±0.08 (RCG) | 1.85 ± 0.13 | 1.90 ± 0.13 | 1.69 ± 0.11 | | |
| 1.6 | $1.86 {\pm} 0.08$ | 1.77 ± 0.10 | 1.84±0.09 (RCG) | 1.73 ± 0.12 | 1.78 ± 0.12 | 1.58 ± 0.13 | | |
| | | | Sum Rate vs. Iteration Rou | ınds | | | | |
| 10 | $30.26 {\pm} 0.33$ | 27.01 ± 0.48 | 29.18±0.36 (P-BF) | 24.88 ± 0.52 | - | 22.48 ± 0.61 | | |
| 30 | 56.13 ± 0.30 | 45.72 ± 0.43 | 55.03±0.32 (P-BF) | 45.16 ± 0.45 | - | 43.19 ± 0.50 | | |
| 50 | 57.85 ± 0.28 | 49.60 ± 0.41 | 57.59±0.29 (P-BF) | 47.51 ± 0.40 | - | 45.34 ± 0.44 | | |
| | Energy Efficiency vs. Iteration Rounds | | | | | | | |
| 10 | $1.47 {\pm} 0.05$ | 1.40 ± 0.06 | 1.42±0.05 (P-BF) | 1.32 ± 0.08 | - | 1.37 ± 0.09 | | |
| 30 | $1.51 {\pm} 0.04$ | 1.44 ± 0.05 | 1.47±0.05 (P-BF) | 1.44 ± 0.08 | - | 1.38 ± 0.07 | | |
| 50 | 1.51 ± 0.04 | 1.44 ± 0.05 | 1.47±0.06 (P-BF) | 1.44 ± 0.09 | - | 1.38 ± 0.08 | | |
| | | | Sum Rate vs. RIS Amplitude I | $Loss(\tau)$ | | | | |
| 0.2 | $18.05 {\pm} 0.36$ | 14.98 ± 0.43 | 12.88±0.48 (FedAvg) | 11.27 ± 0.50 | - | 8.34 ± 0.56 | | |
| 0.6 | 29.21 ± 0.31 | 23.16 ± 0.37 | 22.50±0.42 (FedAvg) | 19.92 ± 0.45 | - | 15.02 ± 0.44 | | |
| 1.0 | 47.28 ± 0.29 | 37.33 ± 0.35 | 35.04±0.39 (FedAvg) | 31.96 ± 0.41 | - | 25.90 ± 0.38 | | |
| | Energy Efficiency vs. RIS Amplitude Loss (au) | | | | | | | |
| 0.2 | $0.71 {\pm} 0.05$ | 0.60 ± 0.05 | 0.52±0.06 (FedAvg) | 0.29 ± 0.08 | - | 0.22 ± 0.10 | | |
| 0.6 | $1.49 {\pm} 0.04$ | 1.21 ± 0.05 | 1.13±0.08 (FedAvg) | 0.92 ± 0.09 | - | 0.61 ± 0.08 | | |
| 1.0 | $1.88 {\pm} 0.05$ | 1.53 ± 0.06 | 1.30±0.07 (FedAvg) | 1.19 ± 0.08 | - | 0.99 ± 0.09 | | |

metrics for model performance. The parameters used in the simulation and their values can be seen in Table I.

To ensure statistical reliability, each simulation was independently executed ten times under random channel realizations. The averaged results of these runs are plotted as line curves in the figures, while the corresponding mean and standard deviation values for all algorithms are summarized in Table II.

B. Simulation on the Number of RIS Reflective Elements

Firstly, we compare the system sum rate under different numbers of RIS reflective elements. In this part of the simulation, the BS transmission power is fixed at 1 W, the number of iterations for FL is set to 50, and we assume the RIS reflective elements do not have reflection amplitude loss. We use the P-BF algorithm proposed in [6] for comparison. Since we are comparing the impact of RIS reflective elements, no simulation without RIS was conducted. As expected, it can be intuitively observed from Fig. 4 that each curve increases as the number of RIS reflective elements increases, leading to a higher system sum rate. As can be observed from the

figure, incorporating FL results in a higher system sum rate compared to the traditional SCA algorithm due to the stopping criteria. With the traditional SCA algorithm, the sum rate essentially reaches its maximum value after 56 RIS reflective elements, while with the SCA-ADMM algorithm and the P-BF algorithm, there are still upward trends in the sum rate when the number of RIS reflective elements reaches 64.

C. Simulation on Transmit Power of the BS

Secondly, we compare the system sum rate and energy efficiency under different BS transmission power levels. In this part of the simulation, the number of RIS reflective elements is fixed at 64, the number of iterations for FL is set to 50, and we assume the RIS reflective elements do not have reflection amplitude loss. We use the RCG algorithm proposed in [11] for comparison. As shown in Fig. 5, under the same conditions, regardless of whether the RIS array is used to reflect signals or whether FL is applied, the proposed SCA-ADMM algorithm is more effective than both the traditional SCA algorithm and the RCG algorithm in enhancing the system sum rate. When both FL and the RIS array are used, even if the BS transmission

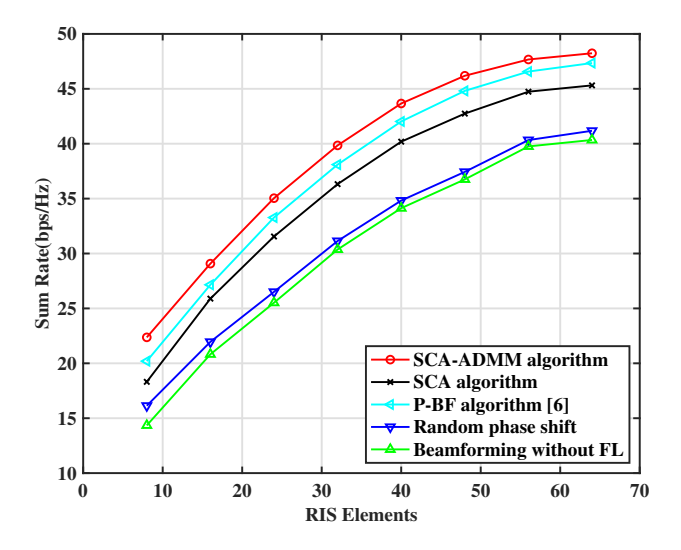


Fig. 4. Sum rate with RIS reflective elements

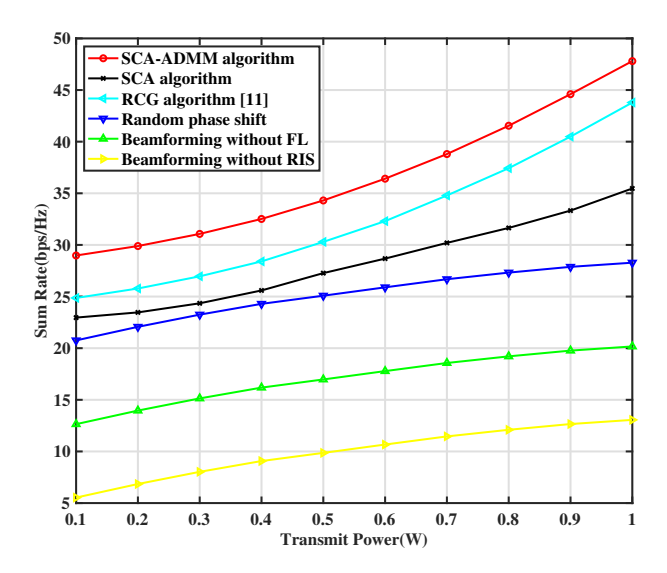


Fig. 5. Sum rate with transmit power of the BS

power increases to 1 W, the system sum rate increases with increasing transmit power. In contrast, when neither RIS nor FL is used, the rate of increase is very slow. It can also be observed that the impact of the RIS array on the system sum rate is greater than that of FL.

In Fig. 6, we compare the system energy efficiency using several beamforming algorithms. The proposed SCA-ADMM algorithm outperforms other algorithms, but has a similar performance to the RCG algorithm. Without FL, the curve of energy efficiency is similar to the one using random phase shift, but much better than the one without RIS. We can see from Fig. 6 that the energy efficiency increases first when the transmit power rises regardless of the beamforming algorithm. When the transmit power reaches 1.2 W, the energy efficiency starts to decrease. This is because when the transmit power is low, the energy efficiency of the system depends on the system

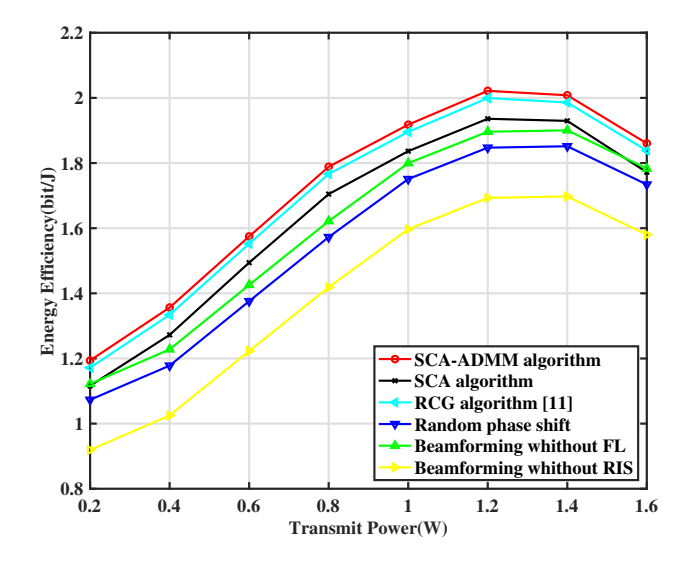


Fig. 6. Energy efficiency with transmit power of the BS

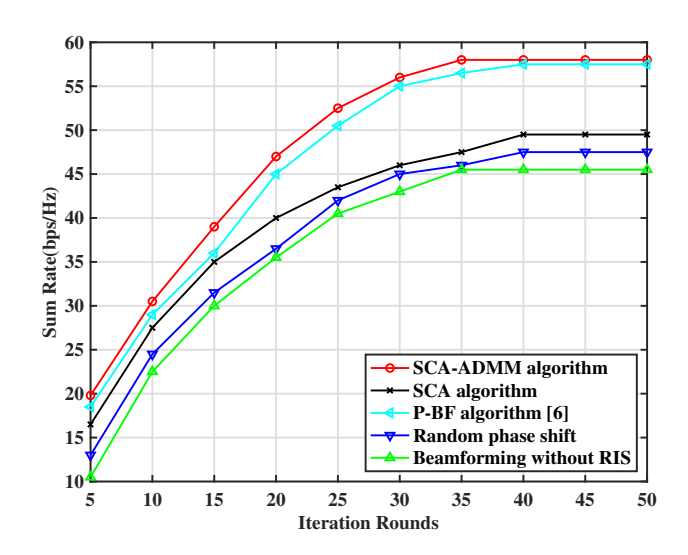


Fig. 7. Sum rate with number of training rounds

sum rate. When the transmit power increases, the power consumption of the system also increases, and the energy efficiency is dependent on the system power consumption.

D. Simulation on the Number of Training Rounds

Next, we compare the system sum rate and energy efficiency under different numbers of FL iterations. In this part of the simulation, the number of RIS reflective elements is fixed at 64, the BS transmission power is set to 1 W, and we assume the RIS reflective elements do not have reflection amplitude loss. We use the P-BF algorithm proposed in [6] for comparison. As shown in Fig. 7, as the number of FL iterations increases, the system sum rate also improves, but it essentially converges when the number of iterations reaches around 40. Additionally, regardless of the presence of the RIS array, the proposed SCA-ADMM algorithm achieves a higher system sum rate than the traditional SCA algorithm, but is

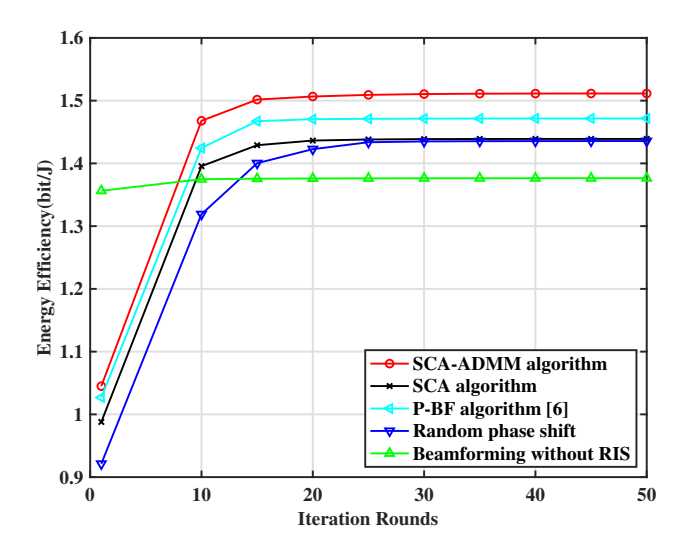


Fig. 8. Energy efficiency with number of training rounds

similar to the P-BF algorithm. In the absence of the RIS array, the performance improvement of the SCA-ADMM algorithm is minimal; however, with the RIS array, it effectively enhances the system sum rate performance. Furthermore, using two RIS arrays to reflect the transmitted signals can more effectively improve the system sum rate.

In Fig. 8, we compare the system energy efficiency using different beamforming algorithms. When the beamforming algorithm has no RIS, the energy efficiency shows little changes regardless of the iteration rounds. All other algorithms converge within 30 rounds of iteration. The proposed SCA-ADMM algorithm outperforms the SCA, the P-BF, and random phase shift beamforming algorithms, as it converges faster and achieves higher energy efficiency under the same number of iteration rounds. The core strength of the proposed algorithm lies in its ability to effectively tackle the highly nonconvex and coupled EE maximization problem by synergistically combining SCA and ADMM. SCA efficiently transforms the non-convex fractional EE objective into a sequence of tractable convex subproblems, allowing us to find a highquality local optimum. Although the SCA algorithm converges faster and achieves better energy efficiency when the number of iteration rounds is low, its performance becomes similar to that of the random phase shift algorithm once both algorithms have converged.

E. Simulation on RIS hardware constraint

Finally, we compare the system performance when the RIS reflective elements have reflecting amplitude loss (i.e., $\tau \leq 1$), which is similar to practical communications. In this part of the simulation, the number of RIS reflective elements is fixed at 64, the BS transmission power is set to 1W, and the number of iterations for FL is set to 50. Meanwhile, we use FedAvg algorithm to show the effectiveness of our proposed method. Fig. 9 illustrates the change of system sum rate when τ rises. Our proposed algorithm consistently achieves the highest sum rate across all τ values, demonstrating its superior capa-

bility in jointly optimizing active and passive beamforming. Furthermore, the monotonically increasing trend of sum rate with higher τ for all RIS-enabled schemes underscores the importance of minimizing RIS hardware imperfections for maximizing system throughput.

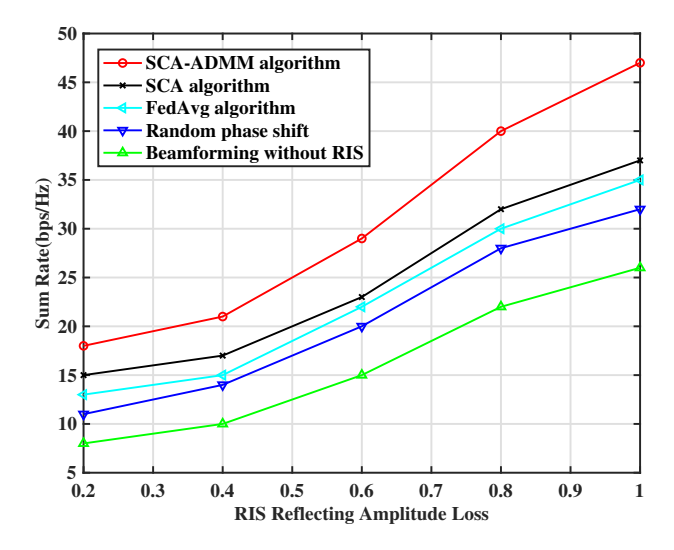


Fig. 9. Sum rate with RIS reflecting amplitude loss

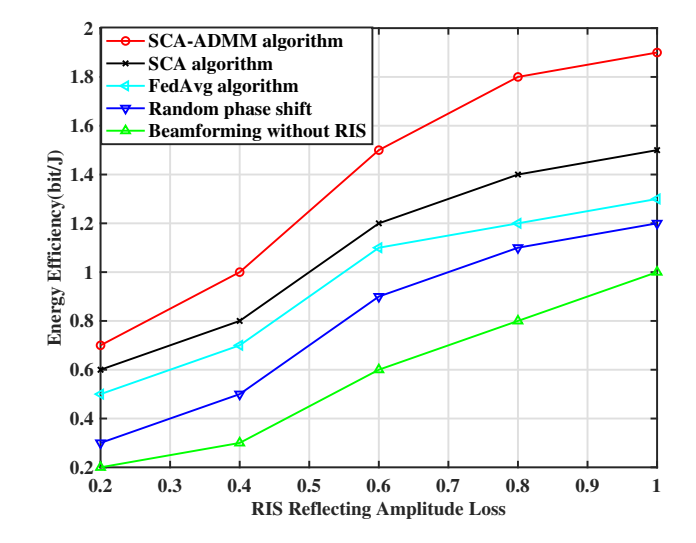


Fig. 10. Energy efficiency with RIS reflecting amplitude loss

Fig. 10 presents the energy efficiency of various algorithms as a function of the RIS reflecting amplitude coefficient. Consistently, all RIS-assisted schemes demonstrate superior energy efficiency compared to the "Beamforming without RIS" baseline, highlighting the substantial benefits of integrating RIS. Our proposed algorithm consistently achieves the highest energy efficiency across the entire range of reflection coefficients. The gradual increase in energy efficiency with improved RIS reflection quality across all curves underscores the critical impact of RIS hardware characteristics on system performance and the necessity for robust optimization algorithms to fully harness its potential.

F. Limitations and Future Works

While our current work presents a robust framework for RIS-empowered FL through an SCA-ADMM co-design, future research could explore several directions to enhance its practicality and scalability in complex real-world scenarios. This includes designing robust resource allocation and FL aggregation mechanisms to ensure consistent performance under dynamic environments with fluctuating device participation and diverse channel conditions.

Furthermore, the current polynomial complexity of our SCA-ADMM approach may pose a bottleneck for extremely large-scale deployments, necessitating the development of more computationally efficient and scalable solutions. A critical future direction also involves extending the framework to jointly optimize resource allocation and RIS configurations for both uplink and downlink transmission phases within each FL communication round, addressing their inherent interplay.

V. CONCLUSION

In this paper, we introduced a novel co-designed framework that tightly integrates FL with RIS-assisted active and passive beamforming to maximize system energy efficiency and sum rate in IoT networks. Our approach goes beyond simple coexistence of FL and RIS; it establishes a bidirectional synergy where RIS dynamically optimizes communication channels for efficient FL data transfer, and the FL process, through its inherent channel-aware weighted aggregation mechanism, intelligently leverages these physical layer enhancements. The proposed SCA-ADMM algorithm effectively solves the complex and highly-coupled joint optimization problem, iteratively optimizing both communication resources and FL parameters to achieve superior performance.

REFERENCES

- X. Yuan, Y. Zhang, Y. Shi, et al., "Reconfigurable-intelligent-surface empowered wireless communications: Challenges and opportunities," *IEEE Wireless Commun.*, vol. 28, no. 2, pp. 136-143, Apr. 2021.
- [2] L. Zhi, H. Niu, Y. He, et al., "Self-powered absorptive reconfigurable intelligent surfaces for securing satellite-terrestrial integrated networks," *China Commun.*, vol. 21, no. 9, pp. 276-291, Sept. 2024.
- [3] A. Chauhan, S. Ghosh, A. Jaiswal, "RIS partition-assisted non-orthogonal multiple access (NOMA) and quadrature-NOMA with imperfect SIC," *IEEE Trans. Wireless Commun.*, vol. 22, no. 7, pp. 4371-4386, July 2023.
- [4] X. Ma, D. Zhang, M. Xiao, et al., "Cooperative beamforming for RIS-aided cell-free massive MIMO networks," *IEEE Trans. Wireless Commun.*, vol. 22, no. 11, pp. 7243-7258, Nov. 2023.
- [5] Q. Wu, R. Zhang, "Intelligent reflecting surface enhanced wireless network via joint active and passive beamforming," *IEEE Trans. Wireless Commun.*, vol. 18, no. 11, pp. 5394-5409, Nov. 2019.
- [6] Q. Tao, S. Zhang, C. Zhong, et al., "Intelligent reflecting surface aided multicasting with random passive beamforming," *IEEE Wireless Commun. Lett.*, vol. 10, no. 1, pp. 92-96, Jan. 2021.
- [7] J. Dang, Z. Zhang, L. Wu, "Joint beamforming for intelligent reflecting surface aided wireless communication using statistical CSI," *China Commun.*, vol. 17, no. 8, pp. 147-157, Aug. 2020.
- [8] E. Bahingayi, K. Lee, "Low-complexity beamforming algorithms for IRS-aided single-user massive MIMO mmwave systems," *IEEE Trans. Wireless Commun.*, vol. 21, no. 11, pp. 9200-9211, Nov. 2022.
- [9] T. Jiang, Y. Shi, "Over-the-air computation via intelligent reflecting surfaces," in *Proc. IEEE Global Commun. Conf. (GLOBECOM)*, Waikoloa, HI, USA, pp. 1-6, Dec. 2019.
- [10] K. An, Y. Sun, Z. Lin, et al., "Exploiting multi-layer refracting RIS-assisted receiver for HAP-SWIPT networks, IEEE Trans. Wireless Commun., vol. 23, no. 10, pp. 12638-12657, Oct. 2024.

- [11] J. An, C. Xu, L. Gan, et al., "Low-complexity channel estimation and passive beamforming for RIS-assisted MIMO systems relying on discrete phase shifts," *IEEE Trans. Commun.*, vol. 70, no. 2, pp. 1245-1260, Feb. 2022.
- [12] Z. Lin, H. Niu, K. An, et al., "Refracting RIS-aided hybrid satellite-terrestrial relay networks: joint beamforming design and optimization," IEEE Trans. Aerosp. Electron. Syst., vol. 58, no. 4, pp. 3717-3724, Aug. 2022.
- [13] X. Ma, Y. Fang, H. Zhang, et al., "Cooperative beamforming design for multiple RIS-assisted communication systems," *IEEE Trans. Wireless Commun.*, vol. 21, no. 12, pp. 10949-10963, Dec. 2022.
- [14] H. Niu, Z. Lin, Z. Chu, *et al.*, "Joint beamforming design for secure RIS-assisted IoT networks," *IEEE Internet Things J.*, vol. 10, no. 2, pp. 1628-1641, Jan. 2023.
- [15] A. Fascista, M. F. Keskin, A. Coluccia, et al., "RIS-aided joint localization and synchronization with a single-antenna receiver: beamforming design and low-complexity estimation," *IEEE J. Sel. Top. Signal Process.*, vol.16, no. 5, pp. 1141-1156, Aug. 2022.
- [16] M. Liu, H. Ren, C. Pan, et al., "Joint beamforming design for double active RIS-assisted radar-communication coexistence systems," *IEEE Trans. Cognit. Commun. Networking*, vol. 10, no. 5, pp. 1704-1717, Oct. 2024.
- [17] Z. Lin, Z. Feng, K. Guo, et al., "AI-driven seamless and massive access in space-air-ground integrated networks," *IEEE Wireless Commun.*, vol. 32, no. 3, pp. 72-79, June 2025.
- [18] C. Wu, F. Wu, L. Lyu, et al., "A federated graph neural network framework for privacy-preserving personalization," *Nature Commun.*, vol. 13, no. 1, June 2022.
- [19] H. Zhang, K. Zeng, S. Lin, "FedUR: federated learning optimization through adaptive centralized learning optimizers," *IEEE Trans. Signal Process.*, vol. 71, pp. 2622-2637, July 2023.
- [20] H. Wu, P. Wang, "Node selection toward faster convergence for federated learning on non-IID data," *IEEE Trans. Network Sci. Eng.*, vol. 9, no. 5, pp. 3099-3111, Sept. 2022.
- [21] J. Chen, J. Li, R. Huang, et al., "Federated transfer learning for bearing fault diagnosis with discrepancy-based weighted federated averaging," *IEEE Trans. Instrum. Meas.*, vol. 71, pp. 1-11, June 2022.
- [22] B. Gu, A. Xu, Z. Huo, et al., "Privacy-preserving asynchronous vertical federated learning algorithms for multiparty collaborative learning," *IEEE Trans. Neural Networks Learn. Syst.*, vol. 33, no. 11, pp. 6103-6115, Nov. 2022.
- [23] G. Zhu, Y. Wang, K. Huang, "Broadband analog aggregation for low-latency federated edge learning," *IEEE Trans. Wireless Commun.*, vol. 19, no. 1, pp. 491-506, Jan. 2020.
- [24] Z. Peng, B. Li, L. Li, et al., "Performance optimization for noise interference privacy protection in federated learning," *IEEE Trans. Cognit. Commun. Networking*, vol. 9, no. 5, pp. 1322-1339, Oct. 2023.
- [25] J. Wang, W. Tang, H. Yu, et al., "Interplay between RIS and AI in wireless communications: fundamentals, architectures, applications, and open research problems," *IEEE J. Sel. Areas Commun.*, vol. 39, no. 8, pp. 2271-2288, Aug. 2021.
- [26] M. Kim, D. Park, "Reconfigurable intelligent surfaces-aided federated learning in over-the-air computation," *IEEE Wireless Commun. Lett.*, vol. 13, no. 7, pp. 1983-1987, July 2024.
- [27] B. Yang, X. Cao, C. Huang, et al., "Federated spectrum learning for reconfigurable intelligent surfaces-aided wireless edge networks," *IEEE Trans. Wireless Commun.*, vol. 21, no. 11, pp. 9610-9626, Nov. 2022.
- [28] A. M. Elbir, S. Coleri, "Federated learning for channel estimation in conventional and RIS-assisted massive MIMO," *IEEE Trans. Wireless Commun.*, vol. 21, no. 6, pp. 4255-4268, June 2022.
- [29] B. Qiu, X. Chang, X. Li, et al., "Federated learning-based channel estimation for RIS-aided communication systems," *IEEE Wireless Commun. Lett.*, vol. 13, no. 8, pp. 2130-2134, Aug. 2024.
- [30] M. A. Cheema, A. Chawla, V. C. Gogineni, et al., "Channel estimation in RIS-aided heterogeneous wireless networks via federated learning", IEEE Commun. Lett., vol. 29, no. 4, pp. 709-713, Apr. 2025.
- [31] Z. Wang, Y. Zhou, Y. Zou, et al., "A graph neural network learning approach to optimize RIS-assisted federated learning," *IEEE Trans. Wireless Commun.*, vol. 22, no. 9, pp. 6092-6106, Sept. 2023
- [32] K. Pillutla, S. M. Kakade, Z. Harchaoui, "Robust aggregation for federated learning," *IEEE Trans. Signal Process.*, vol. 70, pp. 1142-1154, Feb. 2022.
- [33] Y. Cai, S. Li, J. Zhang, et al., "RIS-assisted federated learning algorithm based on device selection and weighted averaging," in Proc. IEEE Veh. Technol. Conf. (VTC2024-Spring), Singapore, Singapore, pp. 1-5, June 2024.

[34] R. Nishihara, L. Lessard, B. Recht, et al., "A general analysis of the convergence of ADMM," in Proc. Int. Conf. on Mach. Learn. (ICML), Lille, France, pp. 343-352, July 2015.



Yujun Cai received his B.S. degree from Communication University of China, Beijing, China, in 2021. He is working toward the Ph.D. in information and communication engineering at the School of Information and Communication Engineering, Communication University of China. His research interests include federated learning and reconfigurable intelligent surface.



Xinruo Zhang received the B.Eng degree in electronics engineering and satellite communications engineering from Beihang University, Beijing, China, in 2010, the M.Sc. degrees in electronics engineering from the University of Surrey, Guildford, U.K., in 2012, and the Ph.D. degree in telecommunications Research from King's College London, London, U.K., in 2018. She is currently a Lecturer with the School of Computer Science and Electronic Engineering, University of Essex, Colchester, U.K. Her research interests include machine learning for

wireless communications, radio resource allocation, and mobile-edge intelligence.



Shufeng Li received the B.Sc. and M.Sc. degrees from Hebei University of Technology, Tianjin, China, in 2004 and 2007, and Ph.D. degree from Beihang University, Beijing, China, in 2011. He is currently a professor with the School of Information and Engineering, Communication University of China, Beijing, China. His research interests mainly include channel estimation, massive MIMO communication, and non-orthogonal multiple access.



Jianbo Liu received the bachelor's degree from the Department of Radio Electronics, Tsinghua University, Beijing, China, in 1985, and the master's degree from the Communication University of China, Beijing, in 1988. He is currently a Professor with the College of Information and Communication Engineering, Communication University of China. His research interests include cable TV and broadband network technology.



Qianyun Zhang received the double B.Sc. degrees in telecommunications engineering from the Beijing University of Posts and Telecommunications, Beijing, China, and the Queen Mary University of London, London, U.K., in 2014, where she is currently pursuing the Ph.D. degree with the School of Electronic Engineering and Computer Science. Her current research interests include characteristic mode analysis, 5G base station antennas, compact UHF and UWB antennas, and their applications on TV white space and M2M/IoT.



Zhijin Qin was with the Imperial College London, Lancaster University, and the Queen Mary University of London, from 2016 to 2022. She is currently an Associate Professor with Tsinghua University. Her research interests include semantic communications and sparse signal processing. She was a recipient of the 2017 IEEE GlobeCom Best Paper Award, the 2018 IEEE Signal Processing Society Young Author Best Paper Award, the 2021 IEEE Communications Society Signal Processing for Communications Committee Early Achievement

Award, and the 2022 IEEE Communications Society Fred W. Ellersick Prize.